Research Article | Vol. 25, No. 9 | 1 May 2017 | OPTICS EXPRESS 10527

Optics EXPRESS

Improving the detection limit for on-chip photonic sensors based on subwavelength grating racetrack resonators

LIJUN HUANG,[1,2,4] HAI YAN,[2] XIAOCHUAN XU,[3,5] SWAPNAJIT CHAKRAVARTY,[3] NAIMEI TANG,[3] HUIPING TIAN,[1,6] AND RAY T. CHEN[2,3,7]

[1]*State Key Laboratory of Information Photonics and Optical Communications, School of Information and Communication Engineering, Beijing University of Posts and Telecommunications, Beijing 100876, China*
[2]*Dept. of Electrical and Computer Engineering, The University of Texas at Austin, Austin, TX 78758, USA*
[3]*Omega Optics Inc., 8500 Shoal Creek Blvd., Austin, TX, 78759, USA*
[4]*hljnet@utexas.edu*
[5]*xiaochuan.xu@omegaoptics.com*
[6]*hptian@bupt.edu.cn*
[7]*raychen@uts.cc.utexas.edu*

Abstract: Compared to the conventional strip waveguide microring resonators, subwavelength grating (SWG) waveguide microring resonators have better sensitivity and lower detection limit due to the enhanced photon-analyte interaction. As sensors, especially biosensors, are usually used in absorptive ambient environment, it is very challenging to further improve the detection limit of the SWG ring resonator by simply increasing the sensitivity. The high sensitivity resulted from larger mode-analyte overlap also brings significant absorption loss, which deteriorates the quality factor of the resonator. To explore the potential of the SWG ring resonator, we theoretically and experimentally optimize an ultrasensitive transverse magnetic mode SWG racetrack resonator to obtain maximum quality factor and thus lowest detection limit. A quality factor of 9800 around 1550 nm and sensitivity of 429.7 ± 0.4nm/RIU in water environment are achieved. It corresponds to a detection limit ($\lambda/S{\cdot}Q$) of 3.71×10^{-4} RIU, which marks a reduction of 32.5% compared to the best value reported for SWG microring sensors.

OCIS codes: (050.6624) Subwavelength structures; (050.2770) Gratings; (280.4788) Optical sensing and sensors; (230.3120) Integrated optics devices.

References and links

1. X. Fan and I. M. White, "Optofluidic microsystems for chemical and biological analysis," Nat. Photonics **5**(10), 591–597 (2011).
2. W. C. Lai, S. Chakravarty, Y. Zou, and R. T. Chen, "Multiplexed detection of xylene and trichloroethylene in water by photonic crystal absorption spectroscopy," Opt. Lett. **38**(19), 3799–3802 (2013).
3. S. Chakravarty, W. C. Lai, Y. Zou, H. A. Drabkin, R. M. Gemmill, G. R. Simon, S. H. Chin, and R. T. Chen, "Multiplexed specific label-free detection of NCI-H358 lung cancer cell line lysates with silicon based photonic crystal microcavity biosensors," Biosens. Bioelectron. **43**, 50–55 (2013).
4. H. Yan, Y. Zou, S. Chakravarty, C. J. Yang, Z. Wang, N. Tang, D. Fan, and R. T. Chen, "Silicon on-chip bandpass filters for the multiplexing of high sensitivity photonic crystal microcavity biosensors," Appl. Phys. Lett. **106**(12), 121103 (2015).
5. Q. Quan, P. B. Deotare, and M. Loncar, "Photonic crystal nanobeam cavity strongly coupled to the feeding waveguide," Appl. Phys. Lett. **96**(20), 203102 (2010).
6. B. H. Ahn, J. H. Kang, M. K. Kim, J. H. Song, B. Min, K. S. Kim, and Y. H. Lee, "One-dimensional parabolic-beam photonic crystal laser," Opt. Express **18**(6), 5654–5660 (2010).
7. K. Yao and Y. Shi, "High-Q width modulated photonic crystal stack mode-gap cavity and its application to refractive index sensing," Opt. Express **20**(24), 27039–27044 (2012).
8. L. Huang, J. Zhou, F. Sun, Z. Fu, and H. Tian, "Optimization of One Dimensional Photonic Crystal Elliptical-Hole Low-Index Mode Nanobeam Cavities for On-chip Sensing," J. Lightwave Technol. **34**(15), 3496–3502 (2016).

#287549 https://doi.org/10.1364/OE.25.010527
Journal © 2017 Received 7 Mar 2017; revised 12 Apr 2017; accepted 22 Apr 2017; published 27 Apr 2017

Optics EXPRESS

9. X. Wang, X. Guan, Q. Huang, J. Zheng, Y. Shi, and D. Dai, "Suspended ultra-small disk resonator on silicon for optical sensing," Opt. Lett. **38**(24), 5405–5408 (2013).
10. S. M. Grist, S. A. Schmidt, J. Flueckiger, V. Donzella, W. Shi, S. Talebi Fard, J. T. Kirk, D. M. Ratner, K. C. Cheung, and L. Chrostowski, "Silicon photonic micro-disk resonators for label-free biosensing," Opt. Express **21**(7), 7994–8006 (2013).
11. X. Fan, I. M. White, H. Zhu, J. D. Suter, and H. Oveys, "Overview of novel integrated optical ring resonator bio/chemical sensors," Lasers Appl. Sci. Eng. 64520M (2007).
12. T. Claes, J. G. Molera, K. De Vos, E. Schacht, R. Baets, and P. Bienstman, "Label-free biosensing with a slot-waveguide-based ring resonator in silicon on insulator," IEEE Photonics J. **1**(3), 197–204 (2009).
13. V. Donzella, A. Sherwali, J. Flueckiger, S. M. Grist, S. T. Fard, and L. Chrostowski, "Design and fabrication of SOI micro-ring resonators based on sub-wavelength grating waveguides," Opt. Express **23**(4), 4791–4803 (2015).
14. L. Huang, H. Tian, J. Zhou, Q. Liu, P. Zhang, and Y. Ji, "Label-free optical sensor by designing a high-Q photonic crystal ring–slot structure," Opt. Commun. **335**, 73–77 (2015).
15. L. Huang, H. Tian, J. Zhou, and Y. Ji, "Design low crosstalk ring-slot array structure for label-free multiplexed sensing," Sensors (Basel) **14**(9), 15658–15668 (2014).
16. C. A. Barrios, "Optical slot-waveguide based biochemical sensors," Sensors (Basel) **9**(6), 4751–4765 (2009).
17. S. Chakravarty, A. Hosseini, X. Xu, L. Zhu, Y. Zou, and R. T. Chen, "Analysis of ultra-high sensitivity configuration in chip-integrated photonic crystal microcavity bio-sensors," Appl. Phys. Lett. **104**(19), 191109 (2014).
18. K. Qin, S. Hu, S. T. Retterer, I. I. Kravchenko, and S. M. Weiss, "Slow light Mach-Zehnder interferometer as label-free biosensor with scalable sensitivity," Opt. Lett. **41**(4), 753–756 (2016).
19. J. T. Kindt, M. S. Luchansky, A. J. Qavi, S. H. Lee, and R. C. Bailey, "Subpicogram per milliliter detection of interleukins using silicon photonic microring resonators and an enzymatic signal enhancement strategy," Anal. Chem. **85**(22), 10653–10657 (2013).
20. S. Schmidt, J. Flueckiger, W. X. Wu, S. M. Grist, S. Talebi Fard, V. Donzella, P. Khumwan, E. R. Thompson, Q. Wang, P. Kulik, X. Wang, A. Sherwali, J. Kirk, K. C. Cheung, L. Chrostowski, and D. Ratner, "Improving the performance of silicon photonic rings, disks, and Bragg gratings for use in label-free biosensing," Proc. SPIE **9166**, 91660M (2014).
21. J. Flueckiger, S. Schmidt, V. Donzella, A. Sherwali, D. M. Ratner, L. Chrostowski, and K. C. Cheung, "Sub-wavelength grating for enhanced ring resonator biosensor," Opt. Express **24**(14), 15672–15686 (2016).
22. X. C. Xu, H. Subbaraman, J. Covey, D. Kwong, A. Hosseini, and R. T. Chen, "Complementary metal–oxide–semiconductor compatible high efficiency subwavelength grating couplers for silicon integrated photonics," Appl. Phys. Lett. **101**(3), 031109 (2012).
23. Z. Wang, X. Xu, D. Fan, Y. Wang, H. Subbaraman, and R. T. Chen, "Geometrical tuning art for entirely subwavelength grating waveguide based integrated photonics circuits," Sci. Rep. **6**(1), 24106 (2016).
24. P. Lalanne and J. P. Hugonin, "High-order effective-medium theory of subwavelength gratings in classical mounting: application to volume holograms," J. Opt. Soc. Am. A **15**(7), 1843–1851 (1998).
25. N. Mortensen, S. Xiao, and J. Pedersen, "Liquid-infiltrated photonic crystals: enhanced light-matter interactions for lab-on-a-chip applications," Microfluid. Nanofluidics **4**(1–2), 117–127 (2008).
26. L. C. Andreani, "Photonic bands and radiation losses in photonic crystal waveguides," Phys. Status Solidi, B Basic Res. **234**(1), 139–146 (2002).
27. L. Chrostowski and M. Hochberg, *Silicon Photonics Design*, (Cambridge University, 2015).
28. J. C. Slater, *Microwave electronics* (Van Nostrand, 1950).
29. W. Bogaerts, P. De Heyn, T. Van Vaerenbergh, K. De Vos, S. Kumar Selvaraja, T. Claes, P. Dumon, P. Bienstman, D. Van Thourhout, and R. Baets, "Silicon microring resonators," Laser Photonics Rev. **6**(1), 47–73 (2012).
30. L. F. Hoyt, "New table of the refractive index of pure glycerol at 20°C," Ind. Eng. Chem. **26**(3), 329–332 (1934).

1. Introduction

In recent decades, optical resonators based sensors on silicon-on-insulator (SOI) platform have been showing great promise in clinical diagnostic assays and biomarker detection. Various resonance structures have been proposed to optimize the performance of these sensors, including two-dimensional photonic crystal (PhC) micro-cavity resonators [1–4], one dimensional PhC nanobeam resonators [5–8], disk resonators [9, 10], and ring resonators [11–13]. High sensitivity (S) is required in those sensors, which strongly depends on optical loss, light polarization, and the overlap between light and the surrounding material. Several structures and methods have been proposed and demonstrated to enhance the sensitivity. These include ring slot resonators [14, 15], slot waveguides [16], nano-holes [17], low index modes [8], slow light effect [18] and transverse magnetic (TM) guide modes [9, 10].

Recently, silicon photonic micro-ring resonator, a typical photonic sensor, based on the interaction between the evanescent wave and the analyte, has been reported that it can match

Optics EXPRESS

and even exceed the detection limit of ELISA (subpicogram/mL) by applying the nanoparticle-clustering methodology to the micro-ring resonator assay [19]. Thus, the overlap between light and matter is larger and the interaction of light and matter is more intense when the evanescent field penetrates deeper into the cladding. Subwavelength grating (SWG) waveguide consists of periodic silicon pillars with a period smaller than the operating wavelength, which can increase the interaction between light and the cladding materials on the top and side of the waveguide, and the space between the silicon pillars on the light propagation path [13]. Intuitively, silicon photonic micro-ring resonator based on SWG waveguide can enhance the evanescent field with respect to a standard silicon strip waveguide resonator with the same cross-section. Therefore, a higher sensitivity can be expected. However, the increased interaction inevitably causes additional absorption loss by analytes and scattering loss induced by surface roughness in the micro-ring region, and the quality factor (Q) of micro-ring resonator would then deteriorate. As a result, for certain wavelength λ, the intrinsic detection limit (iDL = $\lambda/S{\cdot}Q$), which reflects the detection capability of the change of solution concentration may not be enhanced.

In this paper, in order to enhance the photon-analyte interaction to increase the sensitivity without decreasing the qualify factor, and to minimize the detection of limit, we propose a silicon-based transverse magnetic (TM) mode SWG racetrack resonator (SWGRTR) operating at around 1550 nm. The use of TM mode enlarges the overlap between light and sensing medium, thus enhances the photon-analyte interaction and increases the sensitivity. Taking advantage of racetrack-shape resonator brings flexible control of the coupling strength so that the qualify factor of the resonator can be optimized. The experimental results show that a quality factor of 9800 is achieved in water environment when the coupling length and gap are equal to 6.5 μm and 140 nm, respectively. The bulk sensitivity (S) is ~429.7 nm/RIU (refractive index unit), and the enhanced intrinsic detection limit (iDL) of 3.71×10^{-4} RIU are achieved. The intrinsic detection limit is improved by 32.5% compared to the best value reported for SWG microring sensors [20, 21].

2. Device simulation and analysis

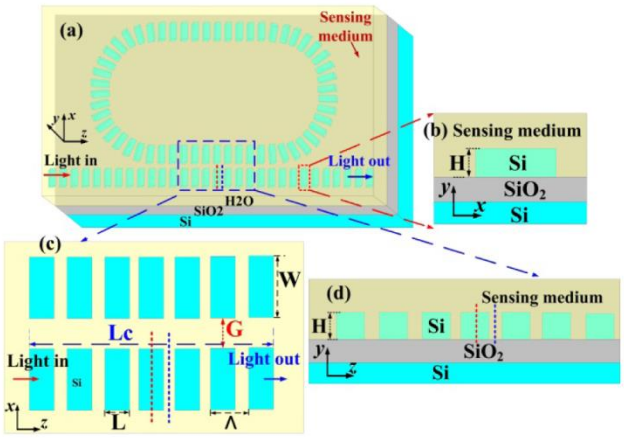

Fig. 1. (a) The schematic of the proposed SWGRTR. (b) The magnified images in *xy* plane in red dashed box. The magnified images of the SWG bus waveguide and the SWG racetrack waveguide in rectangular region with a blue dashed line in (c) *xz* plane and (d) *yz* plane.

A schematic of the proposed SWGRTR is shown in Fig. 1(a). The subwavelength waveguide core is formed by periodically interleaving high refractive index (silicon) and low refractive index (analyte solutions) materials [22, 23]. Figure 1(b) shows the magnified images (*xy* plane) of the pillar region in red dashed box in Fig. 1(a). Figure 1(c) shows the top view (*xz*

Optics EXPRESS

plane) of the coupling region between the bus waveguide and the racetrack resonator in blue box. Figure 1(d) shows a front view (*yz* plane) of the SWG waveguide.

To make the subwavelength waveguide operating in the subwavelength regime ($\lambda/\Lambda > 2n_{eff}$ (λ = 1550 nm)), which does not diffract light in the far field, and propagates between the voids and the silicon blocks (affected by Λ/λ) like the conventional strip waveguide, a period of 200nm is chosen [24]. In Fig. 1(c), Λ represents the period of the SWG structure and equals 200nm. *L*, *W* and *H* are the length, width and thickness of silicon (Si) pillars, respectively. L_c and *G* represent the coupling length and the gap between the bus waveguide and racetrack resonator, respectively. The radius of racetrack is 10μm. The thickness of the buried oxide is 3μm. The upper cladding is the analyte solutions to be detected.

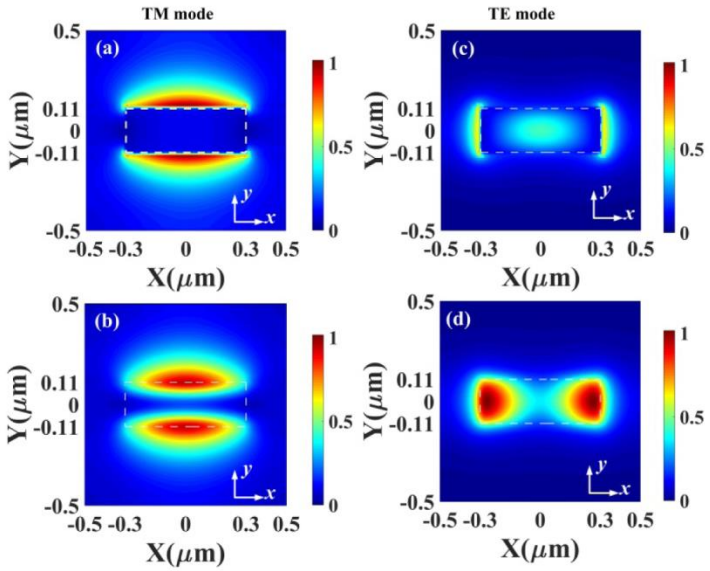

Fig. 2. Electric fields intensity distribution of the TM mode with $L \times W \times H$ of 140 nm × 600nm × 220nm in *xy* plane in red (a) and blue (b) dashed line position in Fig. 1 around 1550 nm. Electric fields intensity distribution of the TE mode with $L \times W \times H$ of 140 nm × 600nm × 220nm in xy plane in red (c) and blue (d) dashed line position in Fig. 1 around 1550 nm.

To analyze the electric field outside Si pillars around 1550 nm, TM mode profiles on *xy* plane at different cutting positions (red and blue dash line in Fig. 1) are simulated in RSoft BandSOLVE and shown in Figs. 2(a) and 2(b). TE mode profiles on *xy* plane at red and blue dash line in Fig. 1 are shown in Figs. 2(c) and 2(d). The dimensions of the silicon pillar in this simulation are *L* = 140 nm, *W* = 600nm, and *H* = 220nm. The Si duty cycle (η) which is defined as the length of silicon (*L*) dividing by period (Λ) is 0.7. As seen in Fig. 2, TM mode electric field extends into the upper cladding and lower substrate in *xy* plane, TE mode electric field extends into the surrounding materials in *xy* plane. It shows that the evanescent field penetrates deeply into the cladding and substrate. The more presence of electrical field in analytes is expected to increase the photon-analyte interaction and subsequently enhance both the bulk and surface sensitivity.

In order to quantify the photon-analyte interaction and the potential of the proposed SWGRTR structure for sensing applications, we calculate the mode volume overlap integral *f* between the optical field and the analytes for TM and TE mode while varying the size of pillars. The overlap integral is defined as [25]:

Optics EXPRESS

$$f = \frac{\int_{V_{low\,index}} \varepsilon \left|\vec{E}\right| dr^3}{\int_{V_{low\,index+dielectric}} \varepsilon \left|\vec{E}\right| dr^3} \quad (1)$$

Here, the volume integral in the numerator is the electric field energy outside of Si pillars. The plot of the f in relation to the duty cycle and width of pillars is shown in Fig. 3(a). The f increases as the Si duty cycle and the width of pillars decrease, meaning the light confinement in the core is decreased and thus the sensitivity is enhanced. However, the optical loss will increase significantly. The photonic modes approach the light line of the cladding materials and are subject to more radiation loss resulting in quasi-guided modes when the waveguide width and Si duty cycle are both located in the green dashed region in Fig. 3(a) [26]. Considering the fundamental mode propagating in the waveguide, we choose a pillar size (η = 0.7, L = 140 nm, W = 600nm, and H = 220nm) labeled in Fig. 3(a) considering the tradeoff between sensitivity and optical loss. The overlap 39.7% of TM modes is larger than 30.2% of TE modes for pillars with the same size. Thus, a higher sensitivity for TM mode SWGRTRs is anticipated compared to the TE mode SWGRTRs with the same geometry.

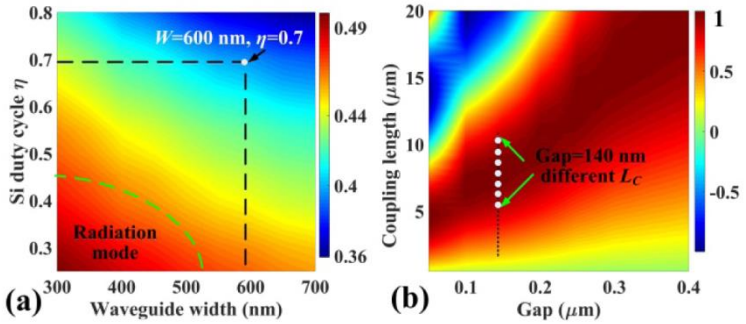

Fig. 3. (a) The plot of the overlap of light and matter changing with the duty cycle and width of Si pillars. (b) The plot of the coupling efficiency changing with the coupling length L_c and the gap G around 1550 nm.

However, the increased interaction inevitably causes additional absorption loss by analytes and scattering loss induced by surface roughness. Therefore, a tradeoff between the photon-analyte interaction and optical loss need to be considered in design. In order to optimize the coupling strength and maximize the quality factor, we analyze the coupling efficiency between the coupling length (L_c) and the gap (G) of the racetrack waveguide and subwavelength bus waveguide with the same dimensions in Fig. 3(a) to minimize the influence of light in the racetrack [27]. We simulate the coupling efficiency shown in Fig. 3(b) changing with L_c and G by RSoft BeamPROP software. The monitors are created to measure the total power along the light propagation direction in the racetrack waveguide. As shown in Fig. 3(b), larger coupling length is needed when the gap increases to achieve a maximum coupling strength from bus SWG waveguide to the racetrack waveguide; because the coupling strength is weakened as the gap is increased. The optimized coupling strength can be satisfied when gap is 140nm and the coupling length is approximately equal to 6μm according to simulations, and thus the maximum quality factor can be expected [28]. Specially, the racetrack resonator becomes a ring resonator when the L_c equals 0. However, the footprint of racetrack resonator is less than that of circular ring resonator with the same circumference.

3. Device fabrication and results

Based on the simulation results in Fig. 3, we fabricated a group of SWGRTRs with different coupling length marked in Fig. 3(b). All devices are fabricated on SOI with a 220nm thick top

Optics EXPRESS

silicon layer and a 3 μm thick buried oxide layer. The SWGRTR structures are firstly patterned with E-beam lithography. The patterns are transferred to the silicon dioxide (SiO_2) hard mask, and then to the silicon layer to form the silicon pillar layer through the reactive-ion-etching. Figure 4(a) shows the optical microscope image of the fabricated SWGRTR with the coupling length of 6.5um, in which light is coupled into the strip waveguide by the TM grating coupler, then coupled into SWG waveguide by the taper, and coupled out by the other taper and grating coupler. Figure 4(b) is the scanning electron microscopy (SEM) image of the fabricated SWGRTR labeled in green dashed rectangular in Fig. 4(a). Figures 4(c), 4(d) and 4(e) are the TM mode grating coupler, the magnified SEM images of the left taper between strip waveguide and SWG waveguide, and the coupling region of the SWG bus waveguide and SWG racetrack waveguide, respectively.

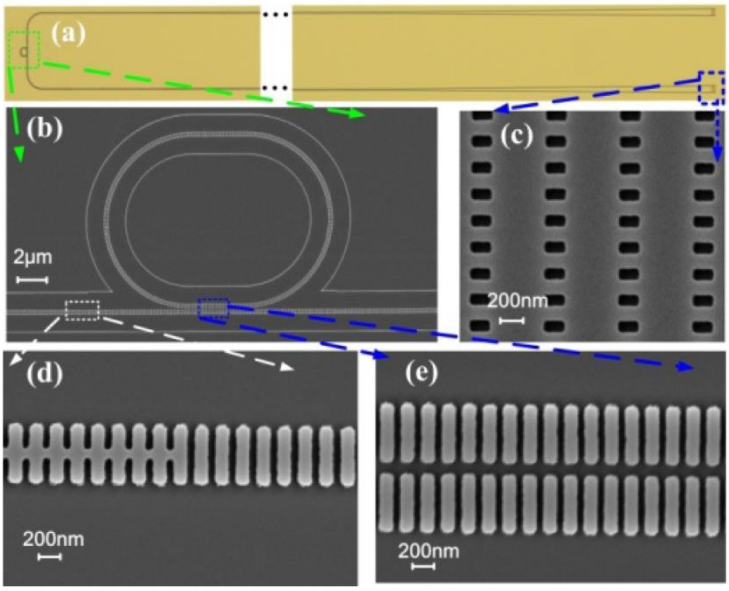

Fig. 4. (a) Optical microscope image of the fabricated SWGRTR with the coupling length of 6.5μm. (b) Scanning electron microscopy (SEM) image of green dashed rectangular region in (a). (c) The TM mode grating coupler in (a). The magnified SEM images of (d) the left taper between strip waveguide and SWG waveguide in white dashed rectangular region, and (e) the coupling region between the SWG bus waveguide and racetrack waveguide in blue dashed rectangular region.

4. Device tests and results

Fabricated devices are tested using a 1550 nm superluminescent LED (SLED) source (covering 1530-1570nm) and an optical spectrum analyzer (OSA). Light from the broadband SLED is guided through one terminal of the fiber array to the TM grating coupler on the chip and excites TM mode in the waveguide. Output light is collected by another terminal of fiber array, and optical spectra are captured by the OSA. The fabricated SWGRTRs with different coupling length are measured in DI water. Figure 5 shows the transmission spectra with 5 different L_c (5.5μm, 6μm, 6.5μm, 7μm, and 7.5μm). Inset in green dashed box shows a magnified view of the resonances in the blue box with each resonance shifted for a relative distance to clarity. As seen in the inset, the quality factor and the extinction ratio of the fabricated SWGRTRs are maximized when the coupling length is 6.5μm. The quality factor of the resonance at 1555.9 nm in DI water is about 9800, and the extinction ratio is about 24.6dB. The optimized coupling length is 6.5μm in fabrication which is slightly different from the simulation results (6 μm). The fabrication induced roughness is possibly the reason for the discrepancy between the simulation and the fabrication. The fabrication results show

Optics EXPRESS

that the fabrication yield of SWG racetrack resonators is better than that of the SWG circular ring resonators due to the large coupling length between the SWG bus waveguide and racetrack waveguide [29].

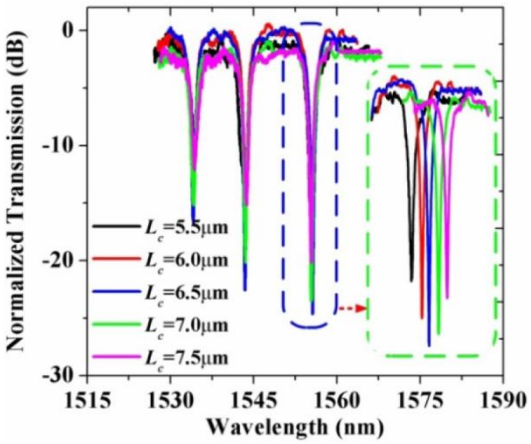

Fig. 5. The testing transmission spectra of the fabricated 5 SWGRTRs with different L_c (5.5μm, 6μm, 6.5μm, 7μm, and 7.5μm) in DI water. Inset in green dashed box is the magnified resonance dips in blue dashed box, and curves were shifted deliberately to show the difference.

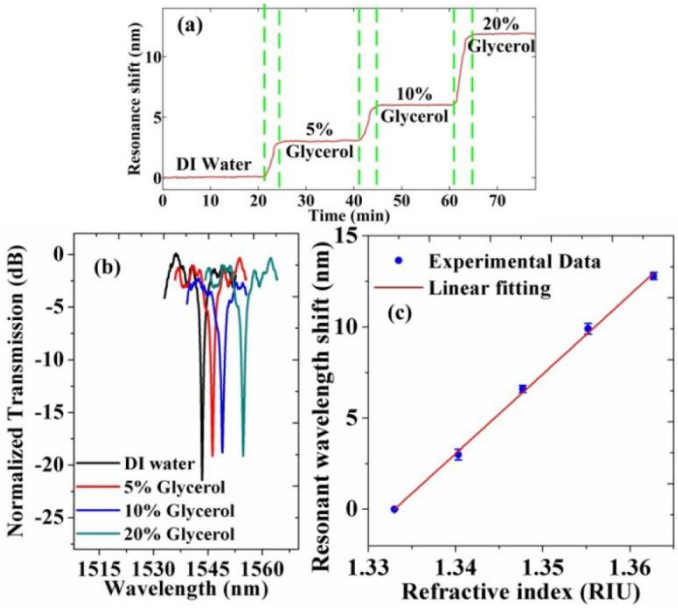

Fig. 6. (a) The results by monitoring the resonance shift for the fabricated SWGRTR with the L_c of 6.5 μm and different concentration glycerol solutions. (b) The corresponding redshift of the transmission spectra for different concentration glycerol solutions (0%, 5%, 10% and 20%). (c) The linear fitting plot of the resonance shifts.

The bulk sensitivity of the fabricated SWGRTRs with different L_c is characterized by monitoring the resonance shift when different concentration solutions are consecutively injected onto the surface of the fabricated samples through microfluidic channels. The chip stage is kept at 25°C with a temperature controller (Newport, Model 3040 Temperature Controller). In order to monitor the performance of the fabricated SWGRTRs, Fig. 6(a) shows the monitoring results of the fabricated SWGRTR with L_c of 6.5μm when solutions with

Optics EXPRESS

different concentration are applied onto the surface of sample. The vertical green dashed line represents the time period when new concentration of glycerol solution is injected and resonance shifts. Figure 6(b) shows the stabilized transmission spectra after the new concentration solutions are applied. The refractive indices for 0%, 5%, 10%, and 20% concentration solutions of glycerol are 1.333, 1.340, 1.347 and 1.362, respectively [30]. Figure 6(c) is the plot of linear fitting of the resonance shift in relation to the change of refractive index of the solution. The bulk sensitivity of the fabricated SWGRTR is about 429.7 ± 0.4nm/RIU.

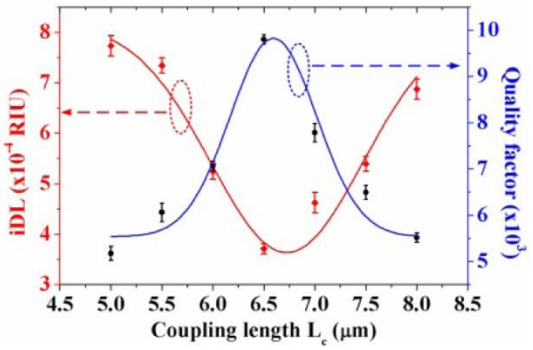

Fig. 7. The *i*DL and quality factor of the fabricated SWGRTRS with different L_c in DI water.

Then, to achieve the detection capability of the change of solution concentration, we analyze the *i*DL. The *i*DL is the minimum index change required to shift the resonance wavelength by one linewidth ($\Delta\lambda_{3dB}$), which is decided by both the sensitivity and the quality factor of resonator. In view of the racetrack resonator with the change of coupling length from 5.5μm to 7.5μm, the bulk sensitivity depends on the mode volume overlap between the optical field and the analytes. The mode volume overlap is the same when only the coupling length is varied and the silicon duty cycle isn't changed, thus the bulk sensitivity is almost the same, whereas the quality factor is a measure of the photon lifetime in the racetrack resonator, which relates to the total loss of resonator and will be changed significantly with the coupling length. Therefore, we optimized the quality factor of racetrack resonator to achieve the lowest *i*DL at maximum *Q*. The *i*DL and quality factor of fabricated SWGRTRs with different L_c are shown in Fig. 7 and fitted with Gaussian curve. It can be seen that the minimum *i*DL and maximum quality factor are achieved simultaneously when the coupling length equals 6.5 μm. At this coupling length, the minimum *i*DL of 3.71×10^{-4} was achieved, which is 32.5% lower than the best value reported in SWG resonator sensor (5.5×10^{-4} RIU) [21]. The sensitivity of the SWGRTR is higher than that of TM mode strip waveguide ring resonators with waveguide thicknesses of 150 nm (247nm/RIU) and 220nm (238nm/RIU) [20].

Moreover, the bulk sensitivity can be further improved by decreasing the Si duty cycle and the width of waveguide to increase the mode volume overlap. However, the optical loss, especially absorption loss and scattering loss, will increase inevitably, which is mentioned in the simulation of overlap in Fig. 3. The absorption loss caused by analytes in water can be suppressed by moving to a shorter wavelength operating at 1310 nm, and the devices would suffer about an order of magnitude less of the absorption loss [20]. The scattering loss can be further decreased if better fabrication condition is available to reduce the surface roughness of devices.

5. Conclusion

In conclusion, we have demonstrated a highly sensitive TM mode SWGRTR without deteriorating the high quality factor to enhance the intrinsic detection limit of sensor. Based on the simulation results, considering the tradeoff between light-analyte interaction and

Optics EXPRESS

optical loss, we choose a pillar size of L = 140 nm, W = 600nm, and H = 220nm. Simulation results show that the mode volume overlap of TM modes is 39.7%, which is larger than the 30.2% of TE modes with the same size of pillars. An optimal Q of 9800 in DI water has been observed when the coupling length, the gap, and silicon duty cycle are equal to 6.5 μm, 140nm, and 0.7, respectively, and the results of bulk index sensing test show a sensitivity of 429.7 ± 0.4nm/RIU. A minimum iDL of 3.71×10^{-4} is achieved and 32.5% lower than that of the circular ring resonator reported recently. In addition, the sensitivity can be further improved by using more aggressive mode volume overlap if better fabrication condition is available.

Funding

Department of Energy (DOE) (contract #: DE SC-0013178). National Cancer Institute/National Institutes of Health (NCI/NIH) (Contract #: HHSN261201500039C). National Natural Science Foundation of China (No. 61372038), Fund of State Key Laboratory of Information Photonics and Optical Communications (Beijing University of Posts and Telecommunications: IPOC2015ZC02), China and Postgraduate Innovation Fund of SICE, BUPT, 2015.

Acknowledgment

Xiaochuan Xu and Ray T. Chen conceived the idea. L. Huang acknowledges the China Scholarship Council (CSC) (NO. 201506470010) for scholarship support.